Applied Catalysis B: Environmental 219 (2017) 683–692

Contents lists available at ScienceDirect

Applied Catalysis B: Environmental

journal homepage: www.elsevier.com/locate/apcatb

Research Paper

Molybdenum-containing systems based on natural kaolinite as catalysts for selective oxidation of aromatic sulfides

Mercedes Muñoz[a,*], María A. Gallo[a,d], Aída Gutiérrez-Alejandre[b], Delia Gazzoli[c], Carmen I. Cabello[a,d]

[a] CINDECA-CCT CONICET La Plata-Universidad Nacional de La Plata, Calle 47 N° 257, 1900, La Plata, Argentina
[b] UNICAT, Departamento de Ingeniería Química, Facultad de Química, UNAM, Cd. Universitaria, 04510, Ciudad de México, Mexico
[c] Dipartimento di Chimica, Univ. di Roma "La Sapienza", Ple. Aldo Moro 5, 00185, Roma, Italy, Italy
[d] CIC-PBA Researcher – Facultad de Ingeniería, UNLP, 1900, La Plata, Argentina

ARTICLE INFO

Article history:
Received 2 March 2017
Received in revised form 19 July 2017
Accepted 1 August 2017
Available online 3 August 2017

Keywords:
Catalysts
Kaolinite
Clean oxidation

ABSTRACT

A natural kaolinite from Argentinean deposits, converted into metakaolin by thermal treatment at 823 K and chemically modified, was used as a support for catalysts containing iso- and heteropolyanions (POMs and HPOMs) such as ammonium heptamolybdate (AHM) and ammonium Anderson phases $[XMo_6O_{24}H_6]^{3-}$ [X(III) = Al, Co]. The catalytic performances were analyzed in the clean selective oxidation of diphenyl sulfide (DPS) with H_2O_2. The chemical modification included treatment in acid solution and functionalization with *3-(aminopropyl)trimethoxysilane* (F). The characterization was carried out by X-ray powder diffraction (XRD), scanning electron microscopy (SEM) with energy dispersive spectrometry (EDS), FTIR and Raman spectroscopies. Textural properties were determined by N_2 adsorption-desorption isotherms (BET method); surface acid properties (Brønsted and Lewis surface acid sites) were measured by FTIR of adsorbed pyridine.

A noticeable increase of surface areas and chemical composition change of the support occurred by acid treatment. Functionalization with amino-siliceous agents yielded an appropriate surface for the adsorption of POMs and HPOMs. The system containing Mo presented conversions of diphenyl sulfide of around 90% and high selectivity to diphenyl sulfone near 95%.

1. Introduction

Kaolinite clays are one of the most important industrial minerals. Due to their physicochemical properties, nontoxicity, low cost, and easy availability, these materials widely applied in geology, agriculture, catalysis, industrial (ceramics, paper, paint, etc.) and environmental processes [1–3]. As for catalysis natural and modified clays find extensive applications in organic reactions. These materials, unlike other conventional catalysts, show considerable advantages such as ease of handling, recyclability, low cost, and easier modulation of acidity levels by suitable exchange of cations, thus contributing to the main subject of "Green Chemistry" [4].

Kaolinites are 1:1 dioctahedral layered materials whose ideal composition is $Al_4Si_4O_{10}(OH)_8$. As a consequence of this structure, they have cationic exchange properties and can intercalate some organic molecules in the interlayer space [5].

The heating of kaolinite between 673 and 973 K involves a dehydroxylation process that produces metakaolinite (MK), an amorphous and more reactive aluminosilicate. The formation of metakaolinite involves a change in the coordination of the Al cations from 6 to 4, and the oxygen atoms bridging two 4-coordinated aluminum atoms may provide the sites needed for hydrogen hopping. Similar mechanisms have been proposed considering the mobility of Si/Al in the solid state [6–9], and might well explain the differences in the reactivity observed among materials with different degrees of structural defects. In ordered kaolinite, the regular stacking produces stronger interlayer contacts and the hydroxyl diffusion process through the interlayer region or at the layer surface requires higher activation energy. In disordered kaolinite, the slight mismatch between adjacent layers due to stacking

* Corresponding author.
E-mail addresses: mmercedes@quimica.unlp.edu.ar, mechemunioz@gmail.com (M. Muñoz).

http://dx.doi.org/10.1016/j.apcatb.2017.08.007
0926-3373/

defects and the relative distortion of the layers, effectively enhance the diffusion of the hydroxyl groups of the two-dimensional particle [10].

The common method of transforming MK into materials active for adsorption and catalysis includes treatments with acidic solutions and chemical modifications [11]. The acid treatment leads to the partial removal of both hydroxyl groups and Al(III) cations and to the enhancement of the Si content. Subsequent chemical modification by various compounds including amino-silane surfactants provides materials with anion/cation exchange properties with specific surface and textural properties [12,13]. All these treatments increase the acidic (Lewis and Brønsted) property of the surface, and it is possible to obtain promising systems for different redox or acid catalytic reactions, such as selective organic oxidation and fine chemistry synthesis [2,14].

The selective oxidation reaction of diphenyl sulfide to obtain sulfoxide/sulfone, using hydrogen peroxide as clean oxidant, is considered a promising alternative to the desulfurization of fuel oil, diesel and H-Bio [15–18]. The great importance of the process in the chemical industry should be highlighted [19]. In comparison with the conventional hydrodesulfurization process (HDS), the ODS can be conducted under less aggressive conditions using simple oxygen carriers such as hydrogen peroxide, which allows working at atmospheric pressure and room temperature, generating water as residue. Sulfoxide and sulfone products have physical and chemical properties that facilitate separation. The reaction efficiency increases notably in the presence of a catalyst. Commonly used catalysts are basically mixed oxides of transition metals supported on various oxidic supports [20–23] though the use of heteropolyacid salts has also been reported [24]. Acid polyoxometalate catalysts are described as efficient for homogeneous ODS, and the performance of meso-structured Ti-MCM-41 catalysts has proven superior to that of conventional MoO_x/γ-Al_2O_3 [25] catalysts. However, many studies indicate a substantial deactivation of catalysts during the reaction. This is often explained as due to the adsorption of the sulfonated substrate on the surface of the solid catalyst. A recent study highlights the effect of the support acidity on the life of molybdenum species supported on Al_2O_3-SiO_2, Al_2O_3-MgO with a variable content of silica and magnesium oxide [26]. According to these studies, the most efficient and long-life catalyst should be a catalyst whose support provides Lewis and Brønsted acid properties. The good performances are attributed to the lack of "leaching" of molybdenum into the reaction medium, which is correlated with the strong substrate-Mo species interaction [27–29].

The use of poly- and heteropolyoxometalates (POMs and HPOMs) in catalysis is limited by their low specific surface area and temperature of decomposition. These species supported on oxide systems (alumina, zirconia, silica or aluminosilicates) become interesting precursors of multimetallic heterogeneous catalysts for a variety of reactions [30–34]. Anderson-type structures (containing Co, Ni or Rh) have recently appeared as interesting heterogeneous catalysts for hydrotreatment and selective hydrogenation processes whereas other POMs, particularly those with Keggin structure, have been successfully applied in several ODS processes [35–38]. The aim of this work was the development a new set of catalysts active in eco-friendly processes combining the versatility of heteropolymolybdates structures (HPOMs, Anderson-type) and the reactivity of widely available and inexpensive clays.

Catalysts with Lewis and Brønsted acidity and redox sites were prepared by grafting Mo-containing POMs and −HPOMs on organosilane functionalized MK surfaces and evaluated in the selective oxidation of diphenyl sulfide to sulfoxide and/or sulfone in the presence of H_2O_2. Their catalytic performances were also compared with results from studies involving more conventional systems.

2. Experimental

2.1. Catalyst preparation

2.1.1. Support preparation

The kaolinite (K) raw material, obtained from an Argentinian deposit (95% of purity), was submitted to thermal treatment in air at 823 K for 2 h to obtain metakaolinite (MK). The material was treated with a H_2SO_4 1:1 solution at 353 K under stirring for 2 h. After separation, the solid was washed with distilled water and dried at 383 K. The product obtained was named MKA.

In order to create new surfaces appropriate for adsorption of both iso- and heteropolyanions, the MKA was functionalized with amino-silane surfactants, according to the following equation:

$$\mathbf{MKAsurface}/(\equiv\mathbf{Si{-}OH})_2 + Si(OMe)_3(CH_2)_3NH_2 \rightarrow MKAsurface/(\equiv Si{-}\mathbf{O})_2Si(OMe)(CH_2)_3NH_2 + 2Me{-}OH \quad (1)$$

The functionalization of MKA was achieved by pretreating MKA with an ethyl alcohol aqueous solution [EtOH:H_2O (50:50)] under continuous stirring at room temperature (24 h) and drying at 353 K (24 h). Subsequently, the solid was contacted with *3-(aminopropyl)trimethoxysilane* (F) in toluene solution under stirring at room temperature for 12 h and subsequently, at 343 K for 12 h. The mixture was filtered, washed with toluene/acetone mixture and vacuum-dried. The product was designated as MKA-F (acid metakaolinite functionalized).

2.1.2. Material synthesis

The MKA and MKA-F materials were impregnated in excess of pore volume with 10 mgMo/mL aqueous solution of (a) $(NH_4)_6[Mo_7O_{24}]\cdot 4H_2O$ (AHM) and (b) Anderson phases $(NH_4)_3[XMo_6O_{24}H_6]\cdot 7H_2O$ (XMo_6, where X(III) = Al, Co). Details on the preparation and characterization of Anderson phases were reported elsewhere [35,36,38].

The Mo content was determined by atomic absorption spectroscopy (AAS), using an IL-457 spectrometer, on initial (C_i) and final (C_f) solutions. The concentration of adsorbed Mo (C_{Mo}) was calculated from experimental C_i (initial) and C_f (final) values, taking into account the volume (V) of impregnating solution and the support mass (m); (mass balance) according to the expression: $Ca = \{[(Ci–Cf) \times V]/m\} \times 100$ [35].

2.2. Characterization of the systems

Surface area measurements, the Brunauer–Emmett–Teller (BET) multipoint method, and textural analysis were performed using Micromeritics ASAP 2020 equipment. The samples were pretreated under vacuum in two stages of 1 h at 373 and 573 K. The mesopore size distribution was determined by the Barrett–Joyner–Halenda (BJH) method from the analysis of the adsorption branch of the isotherm hysteresis; the total pore volume was determined by the rule of Gurvitsch [39–43]. Temperature programmed reduction (TPR) diagrams were obtained in a flow system with a mixture of 10% H_2 volume and 90% Ar volume (10 cm^3/min), by heating from room temperature up to 1123 K at 10 K/min with TCD Shimadzu equipment.

X-ray diffraction patterns (XRD) were obtained with Philips PW 1714 equipment using CuKα (Ni-filtered) radiation in the 2θ range 5°–50°. Scanning electron microscopy (SEM) was performed by a Philips SEM 505 Microscope equipped with dispersive energy system for microanalysis, EDAX 9100.

The acidic properties were analyzed by pyridine adsorption followed by infrared spectroscopy, using a Nicolet 6700 FTIR instrument from Thermo Scientific. A Self-supported wafer of the pure

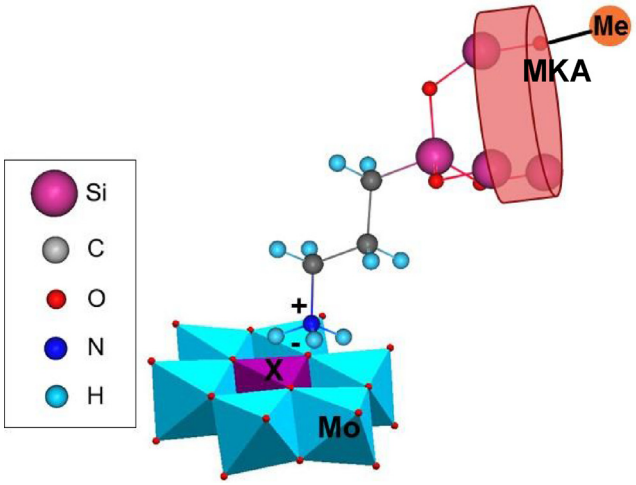

Fig. 1. Ideal representation of XMo_6/MKA-F system.

sample was introduced into a special IR-cell connected to conventional gas manipulation-evacuation equipment and outgassed at 573 K for 3 h. The sample was cooled down to room temperature. Then, a pulse of pyridine was introduced (40 Torr) into the IR-cell, and a spectrum was collected. To eliminate physisorbed pyridine, the sample was outgassed at room temperature and at 423 K for 15 min prior to IR spectra collection. All the measurements were recorded using 4 cm^{-1} resolution and 100 scans per spectrum.

Raman spectra were collected on powder samples at room temperature in the back-scattering geometry with an in via Renishaw spectrometer equipped with an air-cooled CCD detector and edge filters. A 488.0 nm emission line from an Ar^+ ion laser was focused on the sample by a Leica DLML microscope using 5 x or 20 x objectives. The power of the incident beam was about 5 mW. Ten x20 s accumulations were generally acquired for each sample. The spectral resolution was 2 cm^{-1}, and the spectra were calibrated using the 520.5 cm^{-1} line of a silicon wafer.

2.3. Catalytic evaluation

The systems were tested for the oxidation of diphenyl sulfide (DPS) to sulfoxide (DPSO) and/or sulfone ($DPSO_2$) in excess of H_2O_2 as oxidant. The reaction was carried out in batch at 353 K, using 50.0 mg of catalyst, 1 mmol of DPS, 5.0 mL of acetonitrile (solvent of reaction) and 1.0 mL of H_2O_2 35%. For catalytic evaluation, aliquots of 0.2 mL of the reaction mixture were withdrawn at set intervals of time; the organic phase was extracted with dichloromethane/water (1/1) and dried with anhydrous Na_2SO_4.

The catalytic performances were followed by thin layer chromatography (TLC) and gas chromatography (GC), analyzing samples at intervals of 15 min at the beginning of the reaction and of 30 min in the final stage.

The organic phase was analyzed by GC by a Shimadzu 2014 instrument fitted with a 30 m × 0.32 mm SPB-1 capillary column equipped with a FID detector. The GC conditions were the following: initial temperature of 573 K, ramp to 623 K (rate of 5 K/min, temperature constant for 5 min). With this method, the corresponding retention times were: 6.9, 10.5, and 11.1 min for DPS, DPSO, and $DPSO_2$, respectively. The composition of the reaction components was determined by the area normalization method. From these values, the DPS conversion and selectivity values were obtained as a function of time.

The reusability of catalysts was tested for three consecutive cycles. After each use, the catalyst was rinsed with acetonitrile to remove any adsorbed sulfur compounds and dried at 353 K.

3. Results and discussion

3.1. Textural and composition analysis

Thermal and chemical transformation of the original kaolinite, resulting from acid extractive treatment, calcination to 823 K and surface functionalization, yield changes in surface area, porosimetry and chemical composition, Table 1.

Comparison between MK and MKA EDS data indicates that acid leaching leads to an increase of Si content from 63% to 97% due to partial removal of aluminum, in agreement with literature data [44,45].

The increase of BET surface areas, S_{BET}, in the MKA sample corresponds to the formation of mesopore structures (radius ~20 Å according to IUPAC convention) without prevalence of a particular family of pores.

Functionalization of the MKA solid with amino-silane surfactants results in a decrease of the S_{BET} values; however, the external Surface Area was very close to the total area (9.8 m^2/g) resulting in 83.76% of the total area. This effect suggests that the surfactant covered the pores, which is demonstrated by the drastic decrease in the volume of micropores (0.077 cm^3/g). Then the average size value of observable pores corresponds only to meso and macropores [41].

The average pore diameters were 200 and 306 Å for MKA and MKA-F respectively, which according to the classification by

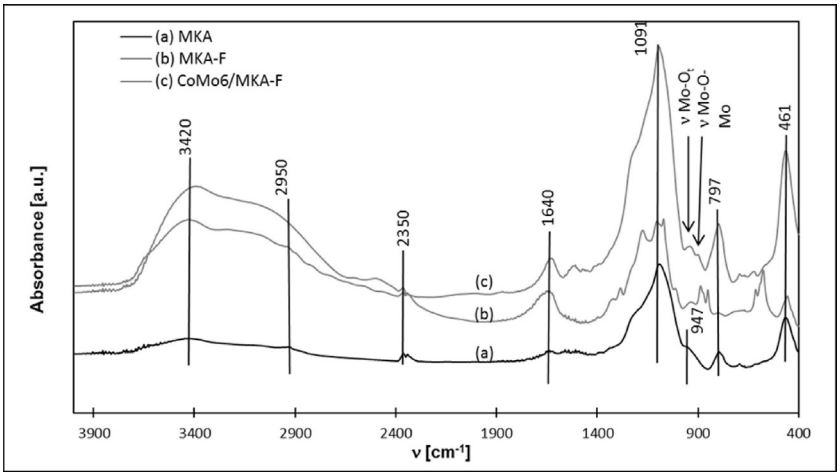

Fig. 2. FTIR comparative spectra of MKA, MKA-F and $CoMo_6$/MKA-F.

Table 1
EDS elemental analysis, surface area and pore parameters values of natural and modified materials.

Supports	% mass			S_{BET} (m^2/g)	Vμpores	Average pore
	C	Si	Al		(cm^3/g)	width(Å)
K	–	69.20	30.80	9.1 (7.06)[a]	0.031	138
MK	–	63.18	36.82	51.0 (35.8)[a]	0.179	168
MKA	–	96.96	3.04	96.0 (73.5)[a]	0.297	200
MKA-F	20.28	77.91	1.81	11.7 (9.8)[a]	0.077	306

[a] Values for external surface area obtained from the t-plot method [41].

Dubinin, correspond to macroporous materials. However, the proportion of super-micropores for MKA was also high [46–48].

The adsorption process of both $(NH_4)_6[Mo_7O_{24}]\cdot 4H_2O$ (AHM) and Anderson phases $(NH_4)_3[XMo_6O_{24}H_6]\cdot 7H_2O$ (XMo_6, where X(III) = Al, Co) on MKA and MKA-F supports occurs mainly by electrostatic interaction [49].

The addition of XMo_6 aqueous solution having a pH of about 5.0 to the MKA or MKA-F materials increases the proton adsorption reaction of the surface —Si—OH groups, forming a positively charged —Si—OH_2^+ unit (MKA surface) and —NH_3^+ (MKA-F surface) [50].

Thus, POM or HPOM molecules containing three negative charges would assemble on the positively charged surface forming anchored XMo_6 clusters [51,52], according to the following surface reactions:

$$\mathbf{3MKAsurface}/[(\equiv\mathbf{Si\text{-}O})_2Si(OMe)(CH_2)_3NH_3]^+: \quad [XMo_6O_{24}H_6]^{3-} + 3NH_4(OH) \qquad (2)$$

where X = Al(III) and Co(III)

An ideal representation of the interaction between one of the negative charges of the Anderson phase (XMo_6) and the MKA-F support is illustrated in Fig. 1.

The MKA-F system shows higher adsorption capacity compared to the non-functionalized one, according to the values of adsorbed Mo (determined by mass balance from AAS data): $AlMo_6$/MKA 0.60%, $AlMo_6$/MKA-F 10.50%, AHM/MKA 0.30%, AHM/MKA-F 10.80%, $CoMo_6$/MKA 1.35% and $CoMo_6$/MKA-F 11.30%.

The X-ray powder diffraction patterns of all samples are similar, showing a prevalent contribution of quartz. It is well-known that under thermal treatment, kaolin transforms into metakaolin, which is an amorphous phase or substantially consists of mullite, according to the reaction occurring in the range 700–900 K: $Al_2Si_2O_5(OH)_4 \rightarrow Al_2O_3\cdot 2SiO_2 + 2H_2O$ [53]. No lines other than those of the supports are detected in the patterns of all the supported systems, indicating the spreading of the different structures containing molybdenum species.

3.2. Analysis by FTIR and Raman spectroscopies

The FTIR spectra for the MKA, MKA-F and $CoMo_6$/MKA-F systems are presented in Fig. 2. The typical aluminosilicate bands dominate all the spectra between 4000 and 400 cm^{-1} with bands associated with the stretching of Al,Si(O) or (T-O-) aluminosilicate bonds located between 900 and 1100 cm^{-1}. For the MKA, Fig. 2a, these bands present a shift to frequencies higher than those expected for MK due to the increase of the relative Si content (Table 1). Upon acidic treatment of MK, a transformation of the tetrahedral sheets to a three-dimensional framework proceeds. The Si–O stretching band is then shifted from the position characteristic for tetrahedral arrangement to sheets in the layer (Fig. 2a) [54]. The bands around 1179 and 1091 cm^{-1} correspond to the asymmetric stretching of the T—O—T bridge, while the symmetric stretching of this group is observed at 797 cm^{-1}. The T—O symmetric stretching is observed at 947 cm^{-1}. The strong band centered at 461 cm^{-1}, ascribed to the angular deformation of the T—O—T bridge, is characteristic of kaoli-

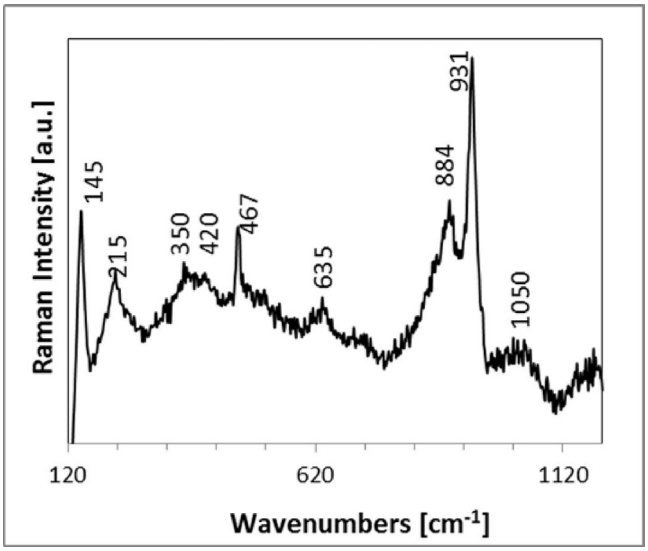

Fig. 3. Micro-Raman spectrum of $AlMo_6$/MKA.

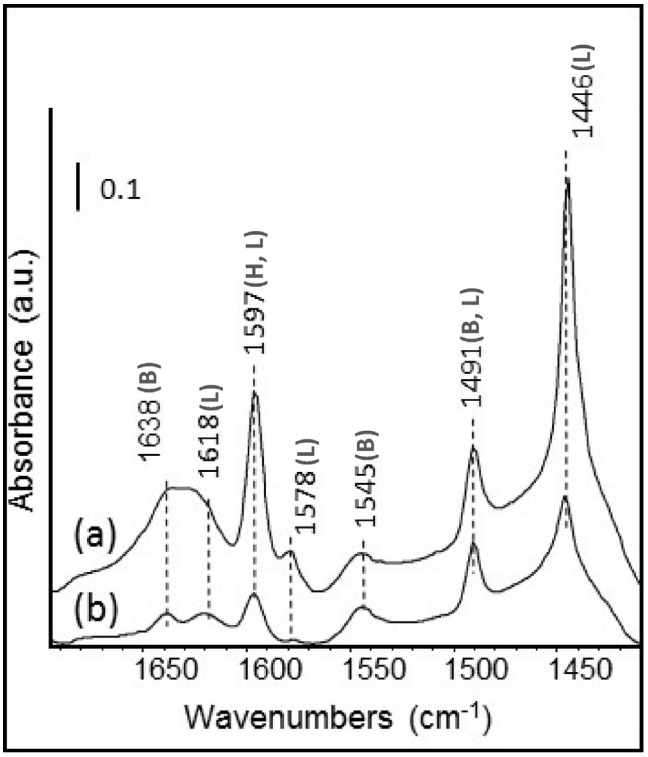

Fig. 4. Comparative FTIR spectra for Py adsorbed on MKA after evacuation: a) at room T and b) at 423 K. (B: Brønsted band; L: Lewis band; and H: hydrogen-bonded Py).

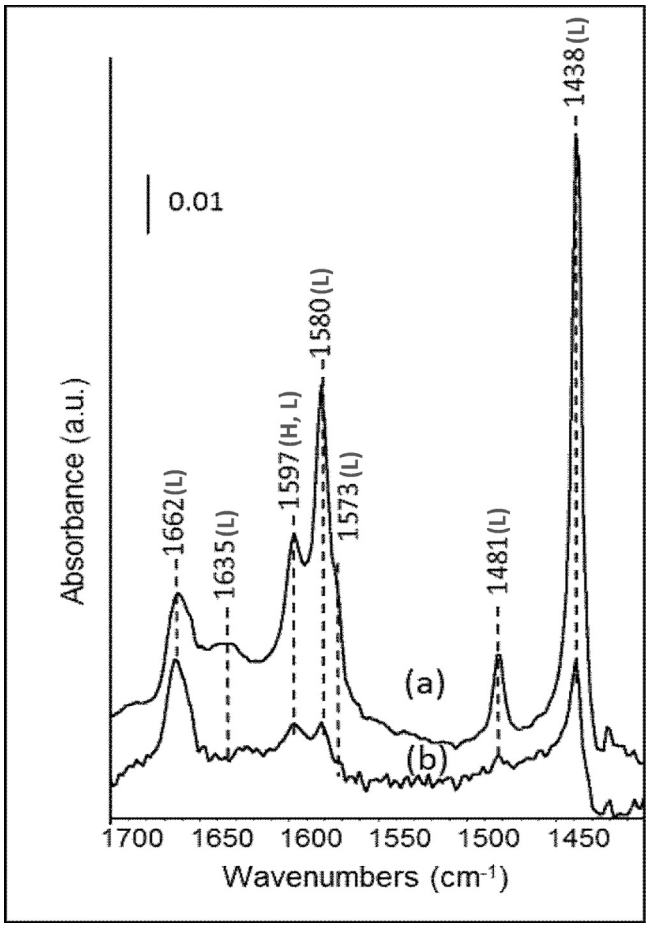

Fig. 5. Comparative FTIR spectra for Py adsorbed on MKA-F after evacuation: a) at room T and b) at 423 K. (B: Brønsted band; L: Lewis band; and H: hydrogen-bonded Py.

nite. Bands corresponding to the stretching of the silanol groups Si/AlO—H, arising from the hydrogen bonded to the silanol groups, in addition to OH stretching bands due to adsorbed water, are observed in the range 3400–2950 cm^{-1}, while the bending modes of water are observed at 1640 cm^{-1}.

The MKA-F FTIR spectrum (Fig. 2b) shows bands associated with the stretching modes of the different functional groups on the surface/$(-Si-O)_2Si(OMe)(CH_2)_3NH_2$ system such as Al,Si (O) groups of aluminosilicate, propylamine $[-(CH_2)_3NH_2]$ and siloxane [—Si—O—Me] [55]. For propylamine $[-(CH_2)_3NH_2]$, the symmetric and asymmetric stretching modes of NH_2 groups are between 3370 and 3300 cm^{-1} overlapped to the high frequency broad band, while the angular deformation of this group appears as part of the strong band at 1650 cm^{-1} due to the bending modes of water. Bands corresponding to the C—N stretching mode and to the N—H out of the plane angular deformation mode appear at 1071 cm^{-1} and at 850 cm^{-1}, respectively.

Furthermore, it is possible to distinguish some characteristic vibrational modes of the siloxane group, such as the [—Si—O—Me] angular deformation mode at 1284 cm^{-1} as well as some angular deformation modes of the $(-CH_n)$ groups between 700 and 672 cm^{-1}.

The FTIR spectra for supported systems also show the main band of the Mo=O bond (~950 cm^{-1}) from POMs and HPOMs [56], Fig. 2c. The Mo-containing molecular units are clearly identified by the Raman microprobe technique. The Raman spectrum of the $AlMo_6$/MKA system in the range 100–1200 cm^{-1} is illustrated in Fig. 3, as a representative case.

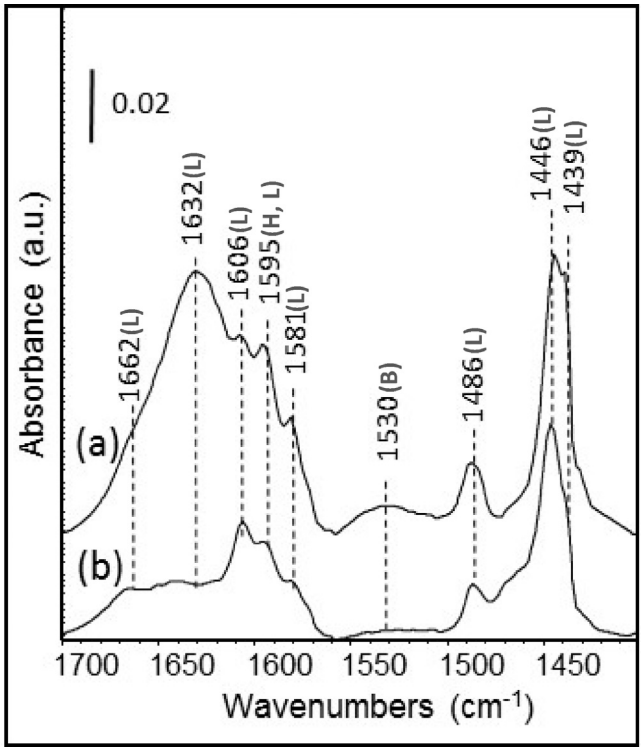

Fig. 6. Comparative FTIR spectra for Py adsorbed on AHM/MKA-F after evacuation: a) at room T and b) at 423 K. (B: Brønsted band; L: Lewis band; and H: hydrogen-bonded Py).

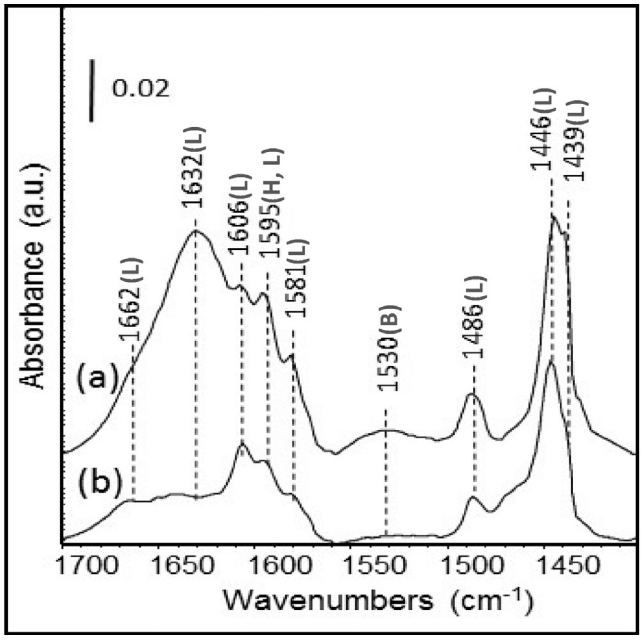

Fig. 7. Comparative FTIR spectra for Py adsorbed on $CoMo_6$/MKA-F after evacuation: a) at room T and b) at 423 K. (B: Brønsted band; L: Lewis band; and H: hydrogen-bonded Py).

Raman bands detected in the $AlMo_6$/MKA sample in the range 100–1200 cm^{-1}, Fig. 3, are due to both the MKA support (100–650 cm^{-1}) and to Mo-containing species (800–1000 cm^{-1}). The Raman identification of the vibrational modes of layered aluminosilicates is not straightforward owing to the complexity of the structural units, variable crystallinity and laser-induced fluorescence. The lattice vibrations are expected to be in the range

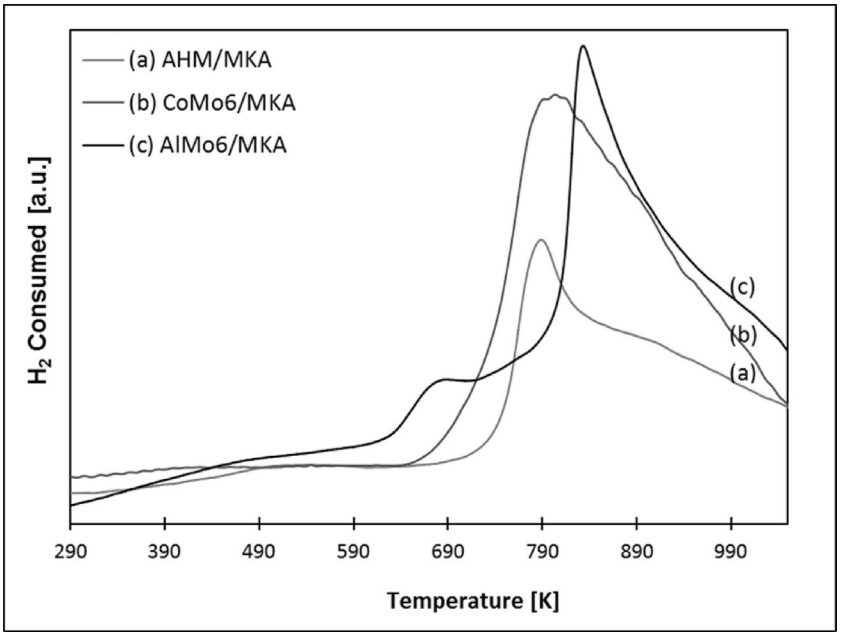

Fig. 8. Comparative TPR patterns for AHM, $AlMo_6$ and $CoMo_6$/MKA supported systems.

Table 2
Concentration of Brønsted, Lewis and total acid sites corresponding to MKA, MKA-F, AHM/MKA-F and $CoMo_6$/MKA-F systems.

	C_L(μmol pyL/gcat)	C_B(μmol pyB/gcat)	C_{total}(μmol/gcat)
MKA	202.35	36.20	238.56
MKA-F	14.78	3.09	17.87
AHM/MKA-F	90.28	2.37	92.66
$CoMo_6$/MKA-F	68.36	18.58	86.93

ε_L = 2.22 cm/μmol, ε_B = 1.67 cm/μmol integrated molar extinction coefficients from Emeis [64].

100–200 cm^{-1} (O—Si—O and O—Al—O symmetric bending modes); vibrations due to the silica and alumina layers, OH bending and charge-balancing cations are in the 200–1300 cm^{-1} spectral range, whereas stretching and bending vibrations of water molecules appear in the range 1600–4000 cm^{-1}.

The Raman band at about 145 cm^{-1} is attributed to the O-Al-O symmetric bend of the AlO_6 group, whereas the bands at about 350, 420, 635 and 1030 cm^{-1} are assigned to the $\nu_2(E)$, $\nu_4(F_2)$, $\nu_1(A_1)$, and $\nu_3(F_2)$ vibrations of the Si—O tetrahedral units [57] in the kaolinite structure. The bands at about 215 and 467 cm^{-1} reveal quartz impurity in kaolin [58].

The band at about 931 cm^{-1} is assigned to Mo=O terminal stretching vibration, whereas the broad feature centered at about 880 cm^{-1} corresponds to Mo—O—Mo bridges in polymolybdate structures.

3.3. Analysis of acid sites by FTIR of absorbed pyridine

To assess the nature of the surface acid sites, FTIR of adsorbed pyridine was determined on the various supported systems.

The infrared bands of pyridine (Py) are commonly designated as “19a”, “19b”, “8a”, and “8b” (following Wilson’s notation [59]), corresponding to the bending and ring-stretching modes. For the coordinative bound Py, these modes are found at about 1447–1460, 1488–1503, 1580, and 1600–1633 cm^{-1}, respectively [59,60]. The Py molecule adsorbed on Brønsted and Lewis acid sites produces bands at about 1540 and 1450 cm^{-1}, respectively [61]. Comparative FTIR spectra (in the region 1700–1400 cm^{-1}) of pyridine adsorption after evacuation at room temperature and at 423 K, together with the main Py band resulting from the adsorption on Brønsted (B) and Lewis (L) acid sites and hydrogen-bonded Py (H) interaction are presented in Figs. 4–7.

For the MKA sample, after evacuation at room T (Fig. 4, curve a), the strong bands at 1446 cm^{-1} and at 1597 cm^{-1} could be related to the adsorption of Py on Lewis acid sites and/or to hydrogen weakly bonded to pyridine molecules [62], whereas the bands at 1545 and 1638 cm^{-1} correspond to Brønsted-bound Py. The band at 1491 cm^{-1} is attributable to the Py molecules adsorbed on both Brønsted and Lewis sites. After outgassing at 423 K (Fig. 4, curve b) there is a significant decrease in the intensity of the bands except the one associated with Brønsted acid sites (1545 cm^{-1}) that preserve its intensity

This profile agrees with those presented by other acid-leached metakaolins [63], confirming the nature of the acid sites of the acid-activated metakaolin.

The spectra of MKA-F support (Fig. 5, curves a and b) differ from those of the MKA one in the absence of the band due to protonated Py (on Brønsted sites, about 1545 cm^{-1}). Bands at 1438 cm^{-1} and at 1481 cm^{-1} are attributed to Py coordinated on Lewis acid sites, whereas the band at 1597 cm^{-1} is assigned to Py interacting with Lewis acid sites and to hydrogen bonding. However, no band of Py on Brønsted acid sites was observed for this system. This behavior suggests that the Brønsted sites could be responsible for the surfactant (F) grafting.

The spectra of AHM/MKA-F (Fig. 6) and $CoMo_6$/MKA-F (Fig. 7) supported systems also present bands attributed to Py coordinated on Lewis acid sites (at 1446, 1457/62 (shoulder), 1606/8, 1628/32 and 1662 cm^{-1}), to Py interacting with Lewis acid sites and hydrogen bonding (~1595/97 cm^{-1}), to hydrogen bonded pyridine adsorbed on surface hydroxyl groups (1439 cm^{-1} and 1581 cm^{-1})

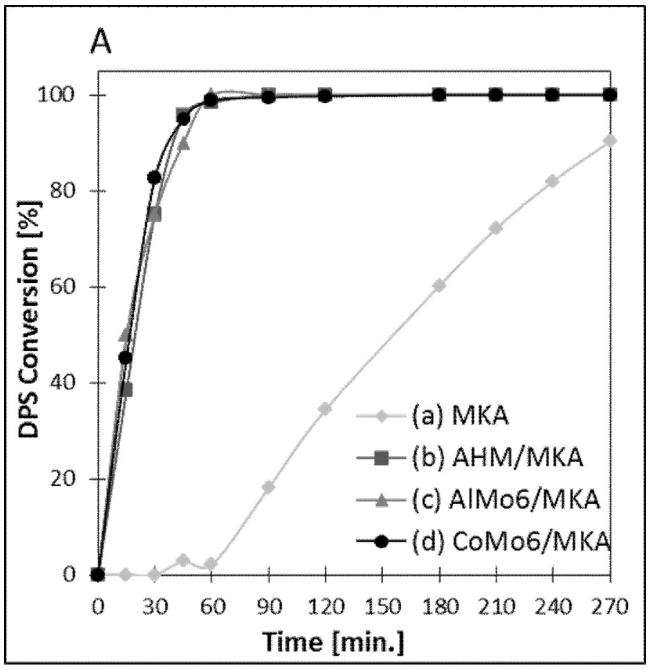

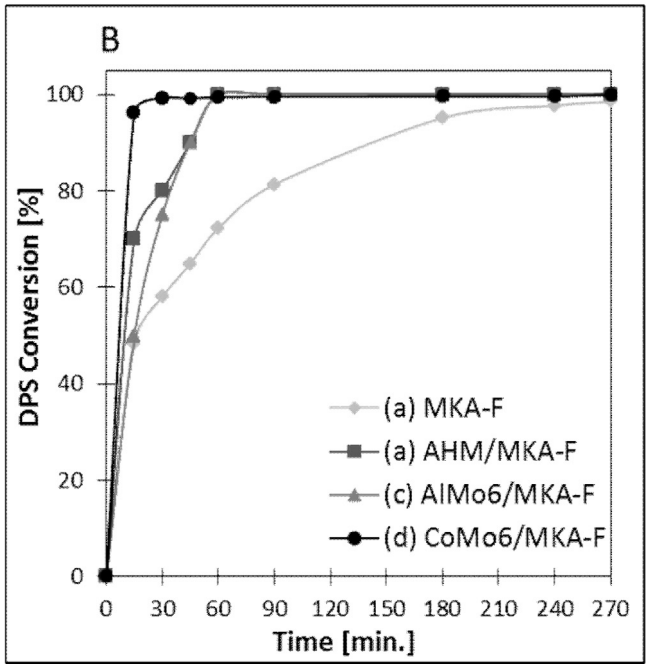

Fig. 9. Conversion (%) as a function of time for the DPS oxidation: (A) MKA and Mo/MKA; (B) MKA-F and Mo/MKA-F systems.

and protonated Py adsorbed on Brønsted acid sites (1530 and 1639 cm^{-1}).

In the spectra of AHM/MKA-F (Fig. 6) and $CoMo_6$/MKA-F (Fig. 7) supported systems outgassed at room temperature, both Brønsted bands at around 1530 and 1630 cm^{-1} and bands at 1460 cm^{-1} due to Lewis acid sites are observed. Outgassing at 423 K markedly changes the FTIR spectra of both AHM/MKA-F and $CoMo_6$/MKA-F supported systems (Figs. 6 and 7, curves b). Bands at around 1439 cm^{-1} and 1606/8 cm^{-1} of Py on Lewis acid sites are observed for these systems, probably due to the less strength of the Lewis acid sites from Mo heteropolymolybdate.

It is well known that the areas of the bands assigned to coordinated pyridine are proportional to the concentration of Lewis

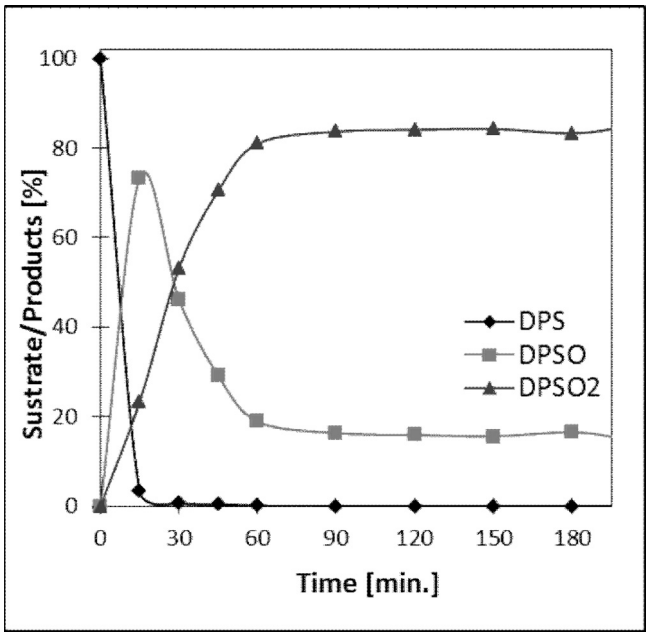

Fig. 10. Time progression of substrate and product concentrations for DPS oxidation catalyzed by $CoMo_6$/MKA-F.

(about 1440 cm^{-1}) and Brønsted (about 1545 cm^{-1}) acid sites [61]. So the intensity of the bands at 1440–48 cm^{-1} corresponds to the total Lewis acid sites, which includes those due to Mo species and to the support, whereas the band at about 1545 cm^{-1} refers to total Brønsted acid sites. Concentration of both, Lewis and Brønsted sites for each catalyst can thus be obtained by the integrated absorbance resulting from curve fitting of the appropriate spectral region using integrated molar extinction coefficients of Py adsorbed on Lewis and Brønsted acid sites (ε_L and ε_B respectively) determined for Emeis on acid sites in Si/Al-based catalysts [64]. The concentration of Brønsted, Lewis and total acid sites for the various catalysts are presented in Table 2.

The results indicate a decrease of total acid sites in the order: MKA > AHM/MKA-F > $CoMo_6$/MKA-F > MKA-F. In the MKA-F systems acid sites are probably masked by the presence of the functionalizing groups on the surface. The increase of Lewis acid sites concentration revealed in the MKA-F systems containing POMs could be due to the presence of Mo.

3.4. TPR analysis

TPR patterns were obtained only for the AHM/MKA and XMo_6/MKA systems to better identify the role of the Mo=O active sites, Fig. 8. Both POM (AHM) and HPOMs ($AlMo_6$ and $CoMo_6$) supported on MKA systems showed the typical signals corresponding to two reduction steps: Mo(VI) → Mo(IV)(673–773 K) and Mo(IV) → Mo° (≈873–973 K), in agreement with the Mo(VI) reduction temperature in Anderson phases and AHM [65,66]. It should be noted that the Mo reduction temperature for the AHM and $CoMo_6$ catalysts was found to be lower than the $AlMo_6$ one and ascribed to the increase in redox stability of Mo in the presence of Al(III) in $AlMo_6$ [65]. On the other hand, compared to alumina or silica carriers, the aluminosilicates cause the activation of the final reduction stage and provide acidic sites that could positively influence a catalytic reaction.

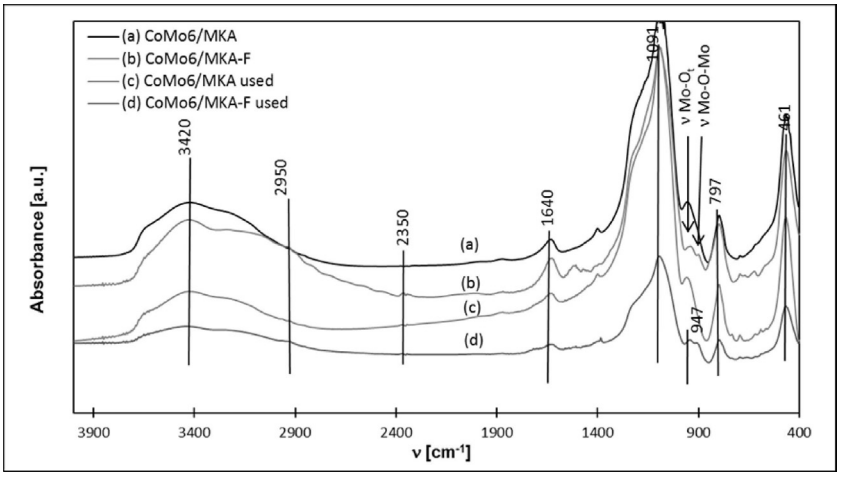

Fig. 11. FTIR comparative spectra of $CoMo_6$/MKA and $CoMo_6$/MKA-F before and after catalytic reaction.

3.5. Catalytic test

Fig. 9 illustrates the results of the conversion of diphenyl sulfide as a function of time, for the MKA and MKA-F bulk and supported systems. MKA-F support (Fig. 9B, curve a) shows a better catalytic behavior than MKA (Fig. 9A, curve a). All Mo-containing systems performed much better (Fig. 9A, curves b-d) or better (Fig. 9B, curves b–d) than the corresponding supports (Fig. 9A and B, curves a).

Furthermore, the Mo-containing systems were selective to sulfone, whereas the MKA and MKA-F supports showed selectivity to sulfoxide, Table 3.

Compared to the catalytic performances exhibited by Mo species on conventional supports in the same experimental condition, our systems were much more efficient for the conversion of diphenyl sulfide. Conversion of 80% was reached in 20 min on $CoMo_6$/MKA-F, whereas on Mo/SiO_2 [21] and on MoO_x/ZrO_2 [22] systems it was reached after 8 h and 2 h, respectively.

Reaction progress for substrate and product concentrations for DPS oxidation in the presence of H_2O_2 is plotted in Fig. 10 for the $CoMo_6$/MKA-F catalyst, as a typical example. This catalytic behavior seems to depend both on the redox properties and on the specific nature of the active acid sites on the catalyst. Redox sites could be identified by the TPR technique, which showed that the Molybdenum reduction temperature was lower for the catalysts exibiting the higher conversion of DPS and selectivity to sulfone. For this reaction, reducibility should be related to the easy formation of peroxo species, as for WO_X supported systems [67] or MoO_x [20].

Regarding acid sites, Brønsted sites are provided by Si—OH— bonds, whereas Lewis sites are generated by both metal-O groups and the functionalizing agent. Although MKA surface presents the highest amount of acid sites, mainly Lewis-type (Table 2), this catalyst led a moderate activity and good selectivity to sulfoxide. It is noticeable that catalysts prepared with the MKA support, having low Mo content (Table 3), resulted in very good activity and selectivity to Sulfone, Fig. 9A.

Practically equivalent catalytic behavior was shown by the XMo_6/MKA-F systems despite the higher Mo concentration and lower amount of Lewis acid sites (Tables 2 and 3). These findings prove that both the synthetic routes are effective in adjusting activity and selectivity and that both procedures generate ordered surfaces with highly available acid and redox sites. It can then be argued that high catalytic performaces can be achieved from the bifunctional contribution of redox properties and Lewis acids sites in the supported catalysts.

In order to check the catalysts reusability some samples were characterizad by FTIR and EDS analysis after removal of sulfur-containing species and then tested for the ODS reaction.

FTIR spectra obtained after reaction for the most active $CoMo_6$/MKA and $CoMo_6$/MKA-F systems are shown as a typical case. A good agreement in the position of the more intense lines was found, denoting the strength of the heteropolyanions-support interaction, Fig. 11. Furthermore EDS analysis on $CoMo_6$/MKA and $CoMo_6$/MKA-F used catalysts revealed no appreciable change in the Co and Mo content, Table 4.

The conversion data for $CoMo_6$/MKA-F before and after three cycles are reported in Table 4.

Results indicate that washing the material for making it recoverable is possible.

A plausible mechanism of the ODS reaction in the presence of H_2O_2 involves the formation of peroxo-molybdate species and the subsequent nucleophilic attack of the sulfur atom in the sulfide on the peroxo species. Indeed, it is known that thioethers are oxidized to sulfoxides by electrophilic oxidants. Mechanistically, it is believed that the electrophilicity of the peroxide oxygen of H_2O_2 is increased by an oxometal group ($Mo{=}O_d$) in the HPOM. As far as H_2O_2 decomposition is concerned, thermal decomposition of H_2O_2 to singlet oxygen $^1O_2$ in water is significant in basic aqueous solution at temperatures above 323 K. Taking into account that the H_2O—H_2O_2 system has a pH < 7 at any H_2O_2 concentration, the decomposition process can be disregarded in our experimental conditions [68].

4. Conclusions

In this work we showed that it is possible to obtain efficient Mo/Co catalysts supporting AHM or Anderson-type heteropolymolybdates $[Al/CoMo_6O_{24}H_6]^{3-}$ on chemically modified and functionalized Argentinean kaolinite (MKA and MKA-F).

The functionalization process led to a support able to anchor polyoxometalate active phases, which provides an interesting approach in the field of immobilized catalysts.

The AHM, XMo_6/MKA and AHM, XMo_6/MKA-F materials, unlike other conventional catalysts, combine the advantages of both polyoxometalates and clays properties, including low cost, wide availability, ease to workup, easy control of metal loading and acidity levels.

The results suggest that deposition of both iso- and heteropolymolybdates as well as the functionalization and subsequent interaction with XMo_6, produces an orderly and sterically convenient MKA surface for the oxidation of aromatic sulphides.

Table 3
Selectivity (%) for supports and catalysts at 1 and 3 h in DPS oxidation.

Catalysts	C_{Mo} %	Selectivity 1 h (%)		Selectivity 3 h (%)	
		DPSO[a]	$DPSO_2$[b]	DPSO[a]	$DPSO_2$[b]
MK	–	84.9	15.0	85.1	14.9
MKA	–	100.0	0.0	96.8	3.2
MKA-F	–	26.5	73.4	27.8	72.1
$AlMo_6$/MKA	0.60	58.8	41.2	8.5	91.5
$AlMo_6$/MKA-F	10.50	4.8	95.2	0.4	99.6
AHM/MKA	0.30	20.3	79.7	0.5	99.5
AHM/MKA-F	10.80	6.1	93.9	0.6	99.4
$CoMo_6$/MKA	1.35	52.1	47.1	1.8	98.1
$CoMo_6$/MKA-F	11.30	18.9	81.1	16.3	83.7

[a] **DPSO:** diphenyl sulfoxide.
[b] **$DPSO_2$:** diphenyl sulfone.

Table 4
Conversion and selectivity (%) for $CoMo_6$/MKA-F systems at 1 h in DPS oxidation for fresh and re-used catalyst (three cycles).

Catalysts	C_{Mo} %	C_{Co} %	Conv. DPS (%) 1h	Selectivity (%) 1 h	
				DPSO[a]	$DPSO_2$[b]
$CoMo_6$/MKA-F	11.30	0.53	100	18.9	81.1
$CoMo_6$/MKA-F Re-used	11.20	0.50	94	21.2	78.8

[a] **DPSO:** diphenyl sulfoxide.
[b] **$DPSO_2$:** diphenyl sulfone.

$CoMo_6$/MKA and $CoMo_6$/MKA-F catalysts were the most active and highly selective to sulfonein the oxidation of diphenyl sulfide with H_2O_2, indicating that the coexistence of both redox and Lewis acid sites is a key point for the catalytic performances.

These preparation methods are an excellent opportunity for building structure-activity relationships among this new family of hybrid materials thus contributing to the design of advanced catalysts.

Acknowledgements

We are grateful to Mrs. Graciela Valle, Eng. Hernán P. Bideberripe, Eng. Edgardo Soto and Lic. Mariela Theiller for their contribution and technical support. The authors would like to thank the following institutions for funding this work: EULALINK Scholarship; MINCYT (Project PICT: 2013/0409); CONICET (Project PIP: 1122011010000); CICPBA (Project 832/14) and Universidad Nacional de La Plata(Project I11/172).

References

[1] R.E. Kirk, D.F. Othmer, Encyclopedia of Chemical Technology, Wiley, New York, 1991.
[2] R.W. Grimshaw, Physics and Chemistry of Clay, fourth ed., Ernest Benn, London, 1971.
[3] W.E. Worral, Ceramic Raw Materials, second ed., Pergamon Press, Leeds, Great Britain, 1982.
[4] P.T. Anastas, M.M. Kirchhoff, T.C. Williamson, Appl. Catal. A: Gen. 221 (2001) 3–13.
[5] L.A.S. do Nascimento, L.M.Z. Tito, R.S. Angélica, C.E.F. da Costa, J.R. Zamiana, G.N. da Rocha Filho, Appl. Catal. B: Environ. 101 (2011) 495–503.
[6] G. Donnay, J. Wyart, G. Sabatier, Z. Kristallogr. 112 (1959) 161–168.
[7] J.R. Goldsmith, D.M. Jenkins, Am. Miner. 70 (1985) 911–923.
[8] J.R. Goldsmith, Contrib. Miner. Petrol. 95 (1987) 311–321.
[9] J.R. Goldsmith, J. Geol. 96 (1988) 109–124.
[10] A. Gualtieri, M. Bellotto, G. Artioli, S.M. Clark, Phys. Chem. Miner. 22 (1995) 215–222.
[11] U. Flessner, D.J. Jones, J. Rozière, J. Zajac, L. Storaro, M. Pavan, A. Jiménez-López, E. Rodríguez-Castellón, M. Trombetta, G. Busca, J. Mol. Catal. A: Chem. 168 (2001) 247–256.
[12] D.M. Araújo Melo, J.A.C. Ruiz, M.A.F. Melo, E.V. Sobrinho, M. Schmall, Micropor. Mesopor. Mat. 38 (2000) 345–349.
[13] J.L. Venaruzzo, C. Volzone, M.L. Rueda, J. Ortiga, Micropor. Mesopor. Mat. 56 (2002) 73–80.
[14] K.R. Sabu, R. Sukumar, R. Rekha, M. Lalithambika, Catal. Today 49 (1999) 321–326.
[15] D.D. Whitehurst, T. Isoda, I. Mochida, Adv. Catal. 42 (1998) 345–471.
[16] D. Wang, E. Weihua Qian, H. Amano, K. Okata, A. Ishihara, T. Kabe, Appl. Catal. A: Gen. 253 (2003) 91–99.
[17] S. Patai, Z. Rappoport, Syntheses of Sulphones, Sulphoxides, and Cyclic Sulphides, Wiley, New York, 1994.
[18] A. Stanislaus, A. Marafi, M.S. Rana, Catal. Today 153 (2010) 1–68.
[19] M. Te, C. Fairbridge, Z. Ring, Appl. Catal. A: Gen. 219 (2001) 267–280.
[20] Z. Ismagilov, S. Yashnik, M. Kerzhentsev, V. Parmon, A. Bourane, F.M. Al-Shahrani, A.A. Hajji, O.R. Koseoglu, Cat. Rev. 53 (2011) 199–255.
[21] J.L. García-Gutiérrez, G.A. Fuentes, M.E. Hernández-Terán, P. García, F. Murrieta-Guevara, F. Jiménez-Cruz, Appl. Catal. A-Gen. 334 (2008) 366–373.
[22] P.S. Raghavan, V. Ramaswamy, T.T. Upadhya, A. Sudalai, A.V. Ramaswamy, S. Sivasanker, J. Mol. Catal A-Chem. 122 (1997) 75–80.
[23] E.P. Polo, C.I. Cabello, D. Gazzoli, Curr. Catal. 3 (2014) 172–178.
[24] V. Rives, M.A. Ulibarri, Coord. Chem. Rev. 181 (1999) 61–120.
[25] A. Chica, A. Corma, M.E. Domine, J. Catal. 242 (2006) 299–308.
[26] V.V.D.N. Prasad, K.E. Jeong, H.J. Chae, C.U. Kim, S.Y. Jeong, Catal. Commun. 9 (2008) 1966–1969.
[27] N. Bejenaru, C. Lancelot, P. Blanchard, C. Lamonier, L. Rouleau, E. Payen, F. Dumeignil, S. Royer, Chem. Mater. 21 (2009) 522–533.
[28] V.C. Srivastava, RSC Adv. 2 (2012) 759–783.
[29] Y. Jia, G. Li, G. Ning, Fuel Process. Technol. 92 (2011) 106–111.
[30] C. Venturello, R. D'Aloisio, J.C.J. Bart, M. Ricci, J. Mol. Catal. 32 (1985) 107–110.
[31] F.P. Ballistreri, G.A. Tomasselli, R.M. Toscano, V. Conte, F.D. Furia, J. Mol. Catal. 89 (1994) 295–301.
[32] L. Salles, C. Aubry, R. Thouvenot, F. Robert, C. Doremieux-Morin, G. Chottard, H. Ledon, Y. Jeannin, J. Bregeault, Inorg. Chem. 33 (1994) 871–878.
[33] L. Salles, C. Aubry, F. Robert, G. Chottard, R. Thouvenot, H. Ledon, J. Bregeault, New J. Chem. 17 (1993) 367–375.
[34] M.T. Pope, A. Müller, Polyoxometalate Chemistry from Topology via Self-assembly to Application, Kluwer Academic Pub London, 2001.
[35] C.I. Cabello, I.L. Botto, M. Muñoz, H.J. Thomas, et al., Catalysts based on $RhMo_6$ Heteropolyoxometalates. Bulk and supported preparation and Characterizatio, in: E. Gaigneaux (Ed.), Studies in Surface Science and Catalysis, Vol. 143, Elsevier Science B.V., 2002, pp. 565–573.
[36] M. Muñoz, M.G. Egusquiza, I.L. Botto, C.I. Cabello, Current Catalysis 3 (2014) 139–146.
[37] M.G. Egusquiza, M. K.B.Tayeb, G. Muñoz, C.I. Romanelli, I.L. Cabello, H.J. Botto, J. Thomas, J. Arg. Chem. Soc. 97 (2009) 166–173.
[38] M. Muñoz, G. Romanelli, I.L. Botto, C.I. Cabello, C. Lamonier, M. Capron, P. Baranek, P. Blanchard, E. Payen, Appl. Catal. B: Environ. 100 (2011) 254–263.
[39] Brunauer, emmett and teller (BET) method, in: J.R. Anderson, K.C. Pratt (Eds.), Introduction to Characterization and Testing of Catalysts, Academic Press, Sydney, 1985.
[40] E.P. Barrett, L.G. Joyner, P.P. Halenda, J. Am. Ceram. Soc. 73 (1951) 373–380.
[41] B.J. Lippens, J.H. de Boer, J. Catal. 4 (1965) 319–323.
[42] W.D. Harkins, G. Jura, J. Am. Ceram. Soc. 66 (1944) 1362–1373.
[43] L. Gurvitsch, J. Phys. Chem. Soc. Russ. 47 (1915) 805–812.
[44] Ch.T. Foo, Ch.S. Mahmood, M.A. Mohd Salleh, Mater. Charac. 62 (2011) 373–377.
[45] M. Lenarda, L. Storaro, A. Talon, E. Moretti, P. Riello, J. Colloid Interf. Sci. 311 (2007) 537–543.

[46] M. Dubinin, Mat. Chem. Rev. 60 (1960) 235–238.
[47] A. Galarneau, A.T. Barodawalla, J. Pinnavaia, Nature 374 (1995) 529–531.
[48] R.S. Murray, J.P. Quirk, Langmuir 6 (1990) 122–124.
[49] A.D. Newman, D.R. Brown, P. Siril, A.F. Lee, K. Wilson, Phys. Chem. Chem. Phys. 8 (2006) 2893–2902.
[50] J. Lu, H. Tang, S. Lu, H. Wu, J.S. Piang, J. Mater. Chem. 21 (2011) 6668–6676.
[51] T. Blasco, A. Corma, A. Martinez, P. Martinez-Escolano, J. Catal. 177 (1998) 306–313.
[52] G. Yadav, N. Asthana, V. Kamble, J. Catal. 217 (2003) 88–99.
[53] K.J.D. Mac Kenzie, I.W.M. Brown, R.H. Meinhold, M.E. Bowden, J. Am. Cer. Soc. 68 (1985) 293–297.
[54] J. Madejova, M. Pentrák, H. Pálková, P. Komadel, Vib. Spectrosc. 49 (2009) 211–218.
[55] B.C. Smith, Infrared Spectral Interpretation: A Systematic Approach, CRC, press, Boca Ratón, 1999.
[56] M. Muñoz, C.I. Cabello, I.L. Botto, M. Capron, C. Lamonier, E. Payen, J. Mol. Struct. 831 (2007) 96–103.
[57] R.L. Frost, Clay Miner. 32 (1997) 65–77.
[58] Y. Liang, C.R. Miranda, S. Scandolo, J. Chem. Phys. 125 (2006) 194524–194532.
[59] M. Castellà-Ventura, Y. Akacem, E. Kassab, J. Phys. Chem. C 112 (2008) 19045–19054.
[60] J.A. Boscoboinik, X. Yu, E. Emmez, B. Yang, S. Yaishalkhutdinov, F.D. Fischer, J. Sauer, H.J. Freund, J. Phys. Chem. C 117 (2013) 13547–13556.
[61] G. Busca, Catal. Today 41 (1998) 191–206.
[62] S.A. Bagshaw, R.P. Cooney, Chem. Mater. 5 (1993) 1101–1109.
[63] M. Perissinotto, M. Lenarda, L. Storaro, R. Ganzerla, J. Mol. Catal. A: Chem. 121 (1997) 103–109.
[64] C.C. Emeis, J. Catal. 141 (1993) 347–354.
[65] C.I. Cabello, I.L. Botto, H.J. Thomas, Thermochim. Acta 232 (1994) 183–193.
[66] C.I. Cabello, I.L. Botto, F. Cabrerizo, M.G. Gonzalez, H.J. Thomas, Adsorpt. Sci. Technol. 18 (2000) 591–608.
[67] G. Rodriguez-Gattorno, A. Galano, E. Torres-García, Appl. Catal. B: Environ. 92 (2009) 1–8.
[68] A.L. Maciuca, C.E. Ciocan, E. Dumitriu, F. Fajula, V. Hulea, Catal. Today 138 (2008) 33–37.